Eur. Phys. J. A manuscript No.
(will be inserted by the editor)

Non-local chiral quark model at finite chemical potential for cold magnetized quark matter

S.A. Ferraris[1], D. Gómez Dumm[2,3], A.G Grunfeld[a,1,2], N.N. Scoccola[1,2]

[1]Departamento de Física, Comisión Nacional de Energía Atómica, Av. Libertador 8250, (1429) Buenos Aires, Argentina
[2]CONICET, Godoy Cruz 2290, Buenos Aires, Argentina
[3]IFLP

Received: date / Accepted: date

Abstract We study the behavior of two-flavor dense quark matter under the influence of an external magnetic field $\vec{B}$, in the framework of an extended, Nambu-Jona-Lasinio model with non-local and separable interactions. This non-locality is incorporated in the model by using a Gaussian form factor. We find that within this model there is a decrease of the critical chiral restoration chemical potential for a rather wide range of increasing magnetic fields.

Keywords First keyword · Second keyword · More

1 Introduction

The phase structure of strongly interacting matter under the influence of an external and uniform magnetic field $\vec{B}$, plays an important role in many applications of theoretical physics such as heavy ion collisions, cosmology and compact star physics. For example, magnetars are compact stars with a strong magnetic field at their surface (expected to be up to $B \backsim 10^{15}\ G$, [1]), and even higher in their interior ([2,3]), where the density could be several times the nuclear saturation density. Quark matter at high densities is expected to be composed of deconfined quarks phases ([4,5]). Then, the study on how features of QCD phase diagram are modified under influence of an external magnetic field became extremely important.

The study of quark matter under extreme conditions of temperature and/or densities involves QCD in the low energy sector, where quantitative calculations are extraordinarily difficult due to its strong coupling. One way to overcome this problem is throughout lattice QCD (lQCD) simulations; however, at finite density they present the harmful sign problem. Then, to circumvent this obstacle, the effective models enter into scene as a powerful tool to describe the strong interacting matter phase diagram at finite densities. It is crucial that effective models show consistency with lQCD simulations at vanishing baryonic chemical potential, before performing extrapolations to higher densities. One of the most widely used chiral quark model model is the Nambu Jona-Lasinio one [6], [7]. In this effective non-renormalizable model, quarks interact in local four point vertices; and a spontaneous chiral symmetry breaking mechanism is included. One characteristic of the NJL model is the lack of confinement, however it can be mimicked throughout the inclusion of the Polyakov loop (PNJL).

In the last decades, some improvements were introduced in the NJL model as covariant non local extensions (nlNJL) [8], [9]. The non local interactions provides the effective model several advantages respect to the local NJL. The inclusion of smooth non local form factors prevents the ultraviolet divergences in momentum space. Moreover, the nlNJL models provide a satisfactory description of the hadron properties at zero temperature and density. Furthermore, the non locality leads to a momentum dependence in quark propagators, consistent with LQCD simulations. A recent detailed review with the description and applications of nlNJL models can be found in [10].

For magnetized quark matter, at zero temperature and vanishing baryonic chemical potential, both, effective models and lQCD agree on the behavior on the chiral condensate, that is an increasing function on the external magnetic field (B). This effect is known as magnetic catalysis (MC) [11]. However, close to the critical chiral restoration temperature (T_c), lQCD simulations predict, for light quark condensates, that T_c decreases with increasing B [12,13]. This effect, known as inverse

[a]e-mail: ag.grunfeld@gmail.com

magnetic catalysis (IMC), is not present in most basic effective models, which close to T_c, predict MC instead. Thus, in this region of the phase diagram, effective models should account for IMC mechanism.

In the present work we are interested in the behavior of cold magnetized strongly interacting matter at finite chemical potential, were diverse studies with effective models were reported in the literature [2,14–19]. In that region, the features of the IMC are different from the above discussed. Here, the critical chemical potential decreases with increasing values of the magnetic fields as was described in Ref. [20]. Even when the NJL model does not show the IMC close to T_c in agreement with lattice simulations, it is observed in at vanishing temperature and finite chemical potential, in the mean field approximation [21–25]. The same effect is obtained when considering quark-quark channels that give rise to two flavour color superconducting quark matter (2SC) [26–29]. As above mentioned, a step further towards a more realistic description of strongly interacting matter in the non perturbative regime, is given by the non local extensions of the NJL model (nlNJL). The nlNJL model, including a coupling to an external static magnetic field, followed by properly implemented Ritus eigenfuncion method, predicts MC for vanishing baryonic chemical potential and low T, and IMC close to T_c [30], in agreement with lQCD simulations. Moreover, beyond mean field level, the nlNJL model successfully describes properties of neutral mesons under the influence of an external magnetic field, at both zero and finite temperature [31], [32].

In the present work we study the behavior of cold strongly interacting matter under a uniform, static magnetic field in the framework of nlNJL model at finite density. Our aim is to extend the previous work [33] to finite density regions and study the corresponding phase diagram for a range of acceptable parameters.

The paper is organized as follows, in Sect. II we describe the theoretical formalism of cold magnetized quark matter within the nlNJL model at finite density. In Sect III we show our results for the chiral limit case and for finite current quark mass. In Sect. IV we present our conclusions.

2 Theoretical formalism

We start by quoting the Euclidean action for the nonlocal chiral quark model under consideration. In the case of two light flavors one has

$$S_E = \int d^4x \, \Big[\bar{\psi}\,(x)\,(-i\partial + m_c)\,\psi\,(x) - \frac{G}{2} j_a\,(x)\, j_a\,(x)\Big] \,, \qquad (1)$$

where ψ stands for the u, d quark field doublet and m_c is the current quark mass, which is assumed to be equal for both quark flavors. The currents $j_a(x)$ are given by

$$j_a\,(x) \;=\; \int d^4z \; \mathcal{G}(z)\,\bar{\psi}\big(x+\frac{z}{2}\big)\Gamma_a\,\psi\big(x-\frac{z}{2}\big) \,, \qquad (2)$$

where we have defined $\Gamma_a = (1, i\gamma_5\vec{\tau})$, and $\mathcal{G}(z)$ is a nonlocal form factor that characterizes the effective interaction.

As we are interested in describing the behaviour of cold and dense magnetized quark matter, we include in the effective action a coupling to an external electromagnetic gauge field $\mathcal{A}_\mu$. For a local theory, this can be done by introducing a covariant derivative in the kinetic term of the action in Eq. (1), i.e. by changing

$$\partial_\mu \;\to\; D_\mu \equiv \partial_\mu - i\hat{Q}\mathcal{A}_\mu\,(x) \,, \qquad (3)$$

where $\hat{Q} = \mathrm{diag}\,(q_u, q_d)$ is the electromagnetic quark charge operator ($q_u = 2e/3$, $q_d = -e/3$). In the case of the nonlocal model studied here, this replacement has to be supplemented by a contribution arising from the nonlocal currents in Eq. (2). One has [34–36]

$$\begin{aligned} \psi\,(x - z/2) \;&\to\; \mathcal{W}\,(x, x - z/2)\;\psi\,(x - z/2) \,, \\ \psi\,(x + z/2)^\dagger \;&\to\; \psi\,(x + z/2)^\dagger\;\mathcal{W}\,(x + z/2, x) \,, \end{aligned} \qquad (4)$$

where the function $\mathcal{W}\,(s,t)$ is defined by

$$\mathcal{W}\,(s,t) \;=\; P\;\exp\left[-i\int_s^t dr_\mu\,\hat{Q}\,\mathcal{A}_\mu\,(r)\right] \,. \qquad (5)$$

Here P stands for path ordering, and r runs over an arbitrary path connecting s with t. As it is usually done, the latter is taken to be a straight line [37]. For simplicity, we restrict to the particular case of a constant and homogeneous magnetic field, which is chosen to be orientated along the 3-axis. To perform the analytical calculations we use the Landau gauge, in which one has $\mathcal{A}_\mu = B\,x_1\,\delta_{\mu 2}$. With this gauge choice the function $\mathcal{W}(s,t)$ in Eq. (5) is given by

$$\mathcal{W}(s,t) \;=\; \exp\left[-\frac{i}{2}\,\hat{Q}\,B\,(s_1 + t_1)\,(t_2 - s_2)\right] \,. \qquad (6)$$

To proceed, we perform a standard bosonization of the theory, introducing scalar and pseudoscalar fields $\sigma(x)$ and $\vec{\pi}(x)$, and integrating out the fermion fields. Moreover, we consider the mean field approximation (MFA), assuming that the field $\sigma(x)$ has a nontrivial translational invariant mean field value $\bar{\sigma}$, while the mean field values of pseudoscalar fields are zero. In the presence of the external magnetic field, it is convenient to write the effective action in a basis of Ritus functions [cita]. Details of this procedure can be found e.g. in Refs. [citas nuestras].

Since we are interested in the study of dense quark matter, we consider a system at nonzero quark chemical potential μ ($\mu = \mu_B/3$, where μ_B is the baryon chemical potential). Then, the grand canonical thermodynamic potential can be obtained from the effective action, including the chemical potential through the replacement $\partial_4 \to \partial_4 - i\mu$ in the kinetic term. In addition, to obtain the appropriate conserved currents, this has to be supplemented by a modification of the nonlocal currents in Eq. (2) [33]. In practice, if the Fourier transform of the nonlocal form factor $\mathcal{G}(z)$ is denoted by $g(p)$, the latter has to be modified by changing $p_4 \to p_4 + i\mu$. In this way, the thermodynamic potential in the MFA is found to be given by

$$\Omega^{\rm MFA}_{\mu,B} = \frac{\bar{\sigma}^2}{2G} - \sum_{f=u,d} \frac{3B_f}{2\pi} \int \frac{d^2p_\parallel}{(2\pi)^2} \times \left[\ln\left(p_\parallel^2 + M_{0,p_\parallel}^{s_f,f\,2}\right) + \sum_{k=1}^{\infty} \ln \Delta^f_{k,p_\parallel} \right] , \quad (7)$$

where

$$\Delta^f_{,p_\parallel} = \left(2kB_f + p_\parallel^2 + M^{+,f}_{k,p_\parallel} M^{-,f}_{k,p_\parallel}\right)^2 + p_\parallel^2 \left(M^{+,f}_{k,p_\parallel} - M^{-,f}_{k,p_\parallel}\right)^2 , \quad (8)$$

with

$$M^{\lambda,f}_{k,p_\parallel} = (1 - \delta_{k_\lambda,-1})\, m_c + \bar{\sigma}\; g^{\lambda,f}_{k,p_\parallel} \quad (9)$$

and

$$g^{\lambda,f}_{k,p_\parallel} = \frac{4\pi}{|q_f B|} (-1)^{k_\lambda} \int \frac{d^2p_\perp}{(2\pi)^2}\; g\left(p_\perp^2 + p_\parallel^2\right) \times \exp\left(-p_\perp^2/B_f\right) L_{k_\lambda}\left(2p_\perp^2/B_f\right) . \quad (10)$$

Here, we use the definitions $p_\perp = (p_1, p_2)$, $p_\parallel = (p_3, p_4 + i\mu)$ and $k_\pm = k - 1/2 \pm s_f/2$, where $s_f = \text{sign}\,(q_f B)$. In addition, we denote $B_f = |q_f B|$, while $L_m\,(x)$ are Laguerre polynomials, with the usual convention $L_{-1}\,(x) = 0$. It can be seen that the functions $M^{\pm,f}_{k,p_\parallel}$ play the role of constituent quark masses in the presence of the external magnetic field. The index k is a quantum number that labels the so-called Landau energy levels of quark fields.

In general, the expression in Eq. (7) turns out to be divergent. It can be regularized following the prescription in Ref. [**?**], namely

$$\Omega^{\rm MFA,reg}_{\mu,B} \;=\; \Omega^{\rm MFA}_{\mu,B} - \Omega^{\rm free}_{\mu,B} + \Omega^{\rm free,reg}_{\mu,B} , \quad (11)$$

where $\Omega^{\rm free}_{\mu,B}$ is a "free" piece obtained from $\Omega^{\rm MFA}_{\mu,B}$ by taking $\bar{\sigma} = 0$ (and keeping the chemical potential and the interaction with the magnetic field). The regularized form of this free piece is given by

$$\Omega^{\rm free,reg}_{\mu,B} = -\frac{N_c}{2\pi^2} \sum_{f=u,d} \Big[B_f^2\; t_f + \sum_k \theta\left(\mu - S_{kf}\right)\; \alpha_k\, B_f\, v_{kf} \Big] , \quad (12)$$

where

$$t_f = \zeta^{'}\left(-1, x_f\right) + \frac{x_f^2}{4} - \frac{1}{2}\left(x_f^2 - x_f\right) \ln x_f \quad (13)$$

and

$$v_{kf} = \mu\sqrt{\mu^2 - S_{kf}^2} - S_{kf}^2\; \ln\left[\frac{\mu + \sqrt{\mu^2 - S_{kf}^2}}{S_{kf}}\right] . \quad (14)$$

Here we denote $x_f = m_c^2/(2B_f)$, $\alpha_k = 1 - \delta_{0k}/2$ and $S_{kf} = \left(m_c^2 + 2kB_f\right)^{1/2}$. In addition, we use the notation $\zeta^{'}\,(z, x_f) = d\zeta\,(z, x_f)\,/dz$, $\zeta\,(z, x_f)$ being the Hurwitz zeta function.

Given the regularized form of the mean field thermodynamic potential, the mean field value $\bar{\sigma}$ can be obtained by solving the gap equation

$$\frac{\partial \Omega^{\rm MFA,reg}_{\mu,B}}{\partial \bar{\sigma}} \;=\; 0 . \quad (15)$$

In general, for each value of μ and B several solutions of this equation may exist. The most stable solution will be the one corresponding to the absolute minimum of $\Omega^{\rm MFA,reg}_{\mu,B}$. Once $\bar{\sigma}$ has been determined, the chiral quark condensates $\langle \bar{q} q \rangle$, with $q = u, d$, can be calculated from

$$\langle \bar{q} q \rangle \;=\; \frac{\partial \Omega^{\rm MFA,reg}_{\mu,B}}{\partial m_q} . \quad (16)$$

3 Numerical results

To obtain the numerical predictions that follow from the formalism described in the preceeding section, it is necessary to specify the particular shape of the nonlocal form factor. In the present work we use a Gaussian function

$$g\left(p^2\right) \;=\; \exp\left(-p^2/\Lambda^2\right) , \quad (17)$$

where Λ is a parameter that indicates the range of the quark level interaction in momentum space. With this particular choice of the form factor, the integral in Eq. (10) can be performed analytically. One gets in this way

$$g^{\lambda,f}_{k,p_\parallel} = \frac{\left(1 - B_f/\Lambda^2\right)^{k_\lambda}}{\left(1 + B_f/\Lambda^2\right)^{k_\lambda + 1}}\; \exp\left(-p_\parallel^2/\Lambda^2\right) . \quad (18)$$

Therefore, the model includes three free parameters, viz. the effective momentum scale Λ, and the constants m_c (current quark mass) and G (coupling constant) that appear in the effective action, Eq. (1). In this work we consider two situations. The first one, discussed in Sec. 3.1, corresponds to the chiral limit, in which we fix $m_c = 0$. Although not really physical, this situation allows for a more clear identification of the possible existing phases and it is, thus, quite useful from a theoretical point of view. The second situation, analyzed in Sec. 3.2, corresponds to the more realistic case in which a finite current quark mass is considered. The way in which the model parameters are determined in each case is discussed in the corresponding subsections.

3.1 Chiral limit

In the chiral limit the number of model parameters reduces to only two, viz. Λ and G. We consider a parametrization in which these are chosen so as to lead to a typical value for the pion decay constant in the chiral limit, $f_{\pi,\mathrm{ch}} = 90$ MeV, and a given value of chiral quark condensate at zero B and μ. To test the sensitivity of our results to the model parameters we consider the cases $-\langle\bar{q}q\rangle_{\mathrm{ch}}^{1/3} = 230$ MeV and 260 MeV. The corresponding parametrizations will be denoted as P230ch and P260ch, respectively. For P230ch we find $\Lambda = 608.3$ MeV and $G\Lambda^2 = 28.43$, while for P260ch the parameter values are found to be $\Lambda = 914.6$ MeV and $G\Lambda^2 = 17.64$.

Given a set of parameters one can numerically solve the gap equation (15) for different values of the chemical potential and the external magnetic field. As mentioned above, for given values of μ and eB this equation has in general more than one solution. In the chiral limit considered in this subsection the solution $\bar{\sigma} = 0$ is always present, while for a fixed value of eB and low enough values of μ a second solution with a nonvanishing value $\bar{\sigma}$ also exists. In particular, for $\mu = 0$ the latter corresponds to the absolute minimum of the thermodynamic potential, implying that the system lies in a phase in which chiral symmetry is spontaneously broken. Now, if one keeps eB fixed and, starting from $\mu = 0$, increases the chemical potential, the value of the thermodynamic potential corresonding to this solution remains unchanged, while that corresponding to the trivial solution $\bar{\sigma} = 0$ is found to decrease, approaching the former. At some critical chemical potential μ_c both values coincide, and for $\mu > \mu_c$ the trivial solution is the one that corresponds to absolute minimum of $\Omega_{\mu,B}^{\mathrm{MFA,reg}}$. Thus, at the critical value $\mu = \mu_c$, which is in general a function of the magnetic field, the system undergoes a transition to a phase in which chiral symmetry is restored.

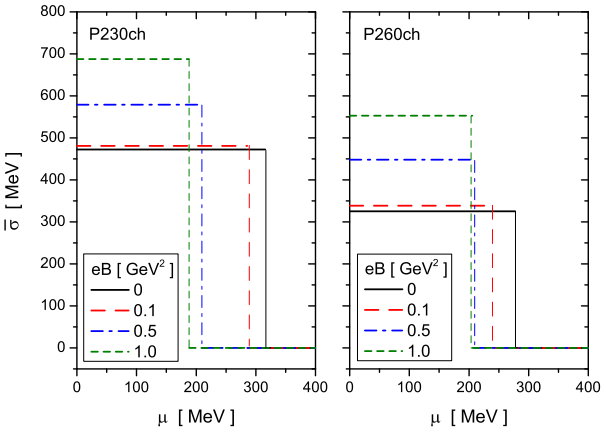

Fig. 1 Mean field value $\bar{\sigma}$ as a function of μ for some selected values of the eB, for parametrizations P230ch (left) and P260ch (right).

The behavior of $\bar{\sigma}$ as a function of μ for some selected values of the magnetic field, and our two parametrizations, is shown in Fig. 1. The vertical lines correspond to the critical chemical potentials μ_c, at which a first order transition is clearly observed. It can be seen that for both parametrizations the value of $\bar{\sigma}$ at $\mu = 0$ gets enhanced if eB is increased. This is a manifestation of the well-known "magnetic catalysis" effect, which entails a growth of the absolute value of the condensate with eB in vacuum. In fact, as shown in Refs. [citas], the rate of this increase is consistent with the results obtained through lQCD simulations [12,13].

It can also be observed that the parametrization choice has some impact on the values of μ_c as well as on their dependence on the magnetic field. To analyze this issue in more detail, in Fig. 2 we plot the value of the critical chemical potential as a function of the parametrization choice, for some selected values of the magnetic field. The parametrization is characterized by the value of $-\langle\bar{q}q\rangle_{\mathrm{ch}}^{1/3}$ in the horizontal axis, which corresponds to a given set of values of Λ and G (the remaining input quantity is, as stated, the value of the pion decay constant, $f_{\pi,\mathrm{ch}} = 90$ MeV). Comparing the results obtained for $eB = 0$ and $eB = 0.01$ GeV^2 (upper panels in Fig. 2) it is seen that although the full line —that corresponds to the first order phase transition between the chiral symmetry broken phase and the chiral symmetry restored phase— is almost identical in both cases, for $eB = 0.01$ the $\bar{\sigma} = 0$ region is subdivided into many phases. Following the notation in Ref. [14], we denote as phase **B** the chiral symmetry broken phase and as $\mathbf{A}_k$ ($k = 0, 1, 2, \dots$) the chiral symmetry restored phases that show up for finite eB. Each one of the latter corresponds to a different num-

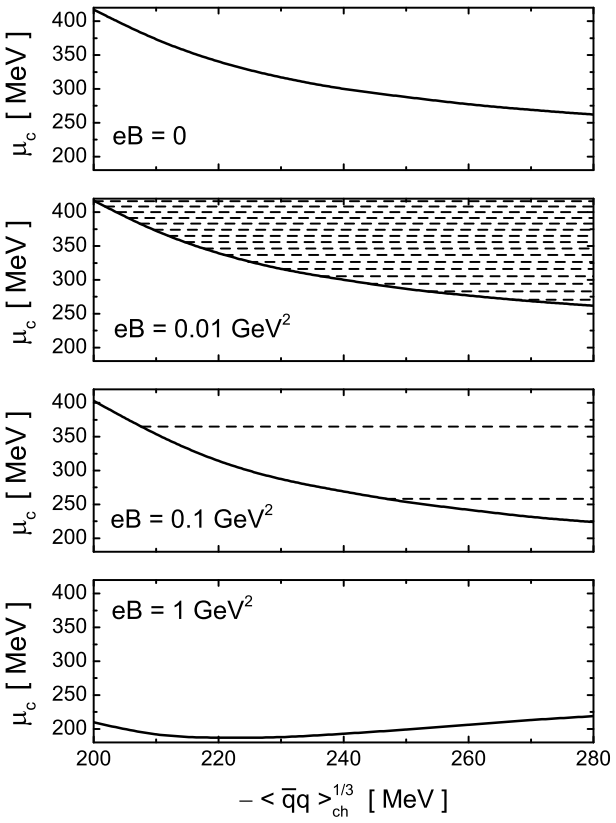

Fig. 2 Critical chemical potential as a function of the parametrization choice, characterized by the value of the quark chiral condensate at zero chemical potential and magnetic field. The graphs correspond to parametrization P230ch and some representative values of eB. The dashed lines indicate the chemical potentials corresponding to the vAdH second order phase transitions.

ber of populated Landau levels, indicated by the index k.

The passage from any of the $\mathbf{A}_k$ phases to the next one is known as a van Alphen-de Haas (vAdH) transition. In the chiral limit discussed in this subsection they are regulated by the Heaviside theta function that appears in the last term of Eq. (12). Hence, the transition form the phase $\mathbf{A}_{k-1}$ to the phase $\mathbf{A}_k$ happens at a critical chemical potential given by

$$\mu_{c,\mathrm{ch}}^{\mathrm{vAdH}} = \sqrt{2kB_f}\ . \tag{19}$$

Clearly, this relation is independent of the parametrization, which explains the fact that in Fig. 2 the dashed lines associated to these transitions are parallel to the horizontal axis. One should keep in mind that in the present case (i.e. for $m_c = 0$) there is no change in the order parameter when one goes from one $\mathbf{A}_k$ phase to the next one. In fact, one has $\bar{\sigma} = 0$ for all these phases, and, consequently, all these transitions are of second order. The effect of vAdH transitions on physical quantities can be seen, for example, in the quark density $\rho_q = -\partial\Omega_{\mu,B}^{\mathrm{MFA,reg}}/\partial\mu$. This is illustrated in

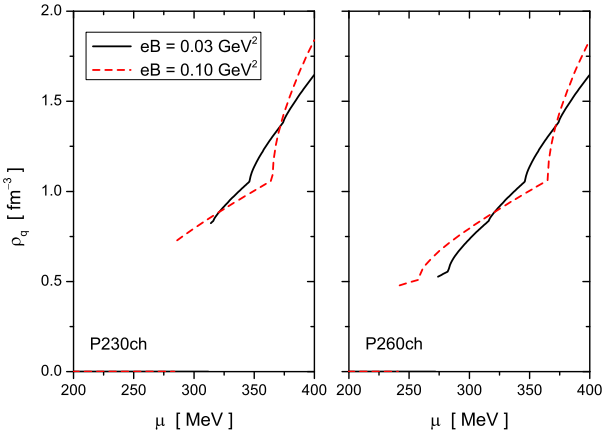

Fig. 3 Quark density as a function of the quark chemical potential, for two representative values of eB and parametrizations P230ch (left) and P260ch (right).

Fig. 3, where we show the behavior of ρ_q as a function of μ for two representative values of the magnetic field and both parametrizations P230ch and P260ch. It can be observed that when the system moves from a given phase $\mathbf{A}_k$ to the next one the derivative of the density shows a discontinuity at the transition point.

As it follows from Eq. (19), the number of vAdH transitions in a certain range of chemical potentials depends on the magnetic field strength. This is the reason why in the panel corresponding to $eB = 0.01$ GeV^2 one observes a quite large number of vAdH transitions, while for $eB = 0.1$ GeV^2 there are only two, and none is found for $eB = 1$ GeV^2.

Another interesting point to be observed in Fig. 2 is that the dependence of the critical chemical potential for the first order transition with the parametrization (solid lines) is quite similar for $eB = 0$, 0.01 GeV^2 and 0.1 GeV^2. In all these cases the value of μ_c decreases as the (absolute) value of the condensate that characterizes the parametrization increases. However, for $eB =$ 1 GeV^2 the situation is different. For parametrizations corresponding to $-\langle\bar{q}q\rangle_{\mathrm{ch}}^{1/3} \gtrsim 220$ MeV we find that μ_c slightly increases with the absolute value of the condensate. Thus, one can expect that for large values of eB the behaviour of μ_c would be more sensitive to the chosen parametrization.

In addition, it is important to remark that for the whole range of parametrizations considered in the present nonlocal model one finds a direct transition from the phase $\mathbf{B}$ to any of the phases $\mathbf{A}_k$. This differs from the situation observed for the case of the local NJL

model, in which for some parametrizations one finds intermediate massive phases $\mathbf{C}_k$ [22].

We finish this subsection by considering the phase diagrams of magnetized cold quark matter in the $eB-\mu$ plane for parametrizations P230ch and P260ch, shown in Fig. 4. As stated, **B** denotes the spontaneous chiral

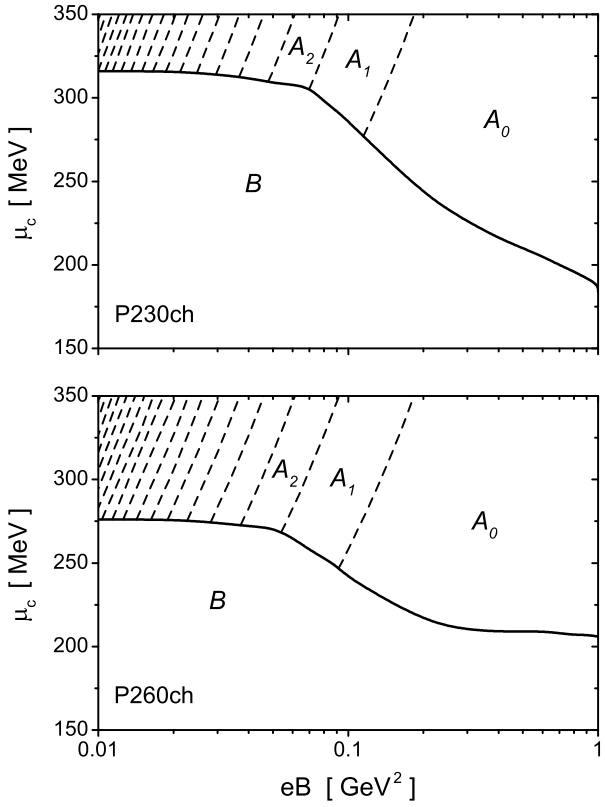

Fig. 4 Phase diagrams in the $eB-\mu$ plane in the chiral limit case, for parametrizations P230ch (up) and P260ch (down). Solid and dashed lines correspond to first and second order phase transitions, respectively.

symmetry broken phase, while $\mathbf{A}_k$ correspond to chiral symmetry restored phases. The second order transitions between $\mathbf{A}_k$ phases are indicated by the dashed lines. Each time one of these lines is crossed from right to left, new Landau levels get populated. The crossing from $\mathbf{A}_0$ to $\mathbf{A}_1$ corresponds to the population of the d-quark state with $k = 1$, while for the u-quark state only the lowest level $k = 0$ is allowed. Then, the crossing from $\mathbf{A}_1$ to $\mathbf{A}_2$ implies the simultaneous population of the u-quark state with $k = 1$ and the d-quark state with $k = 2$, etc. The fact that the population of the up quark state with a certain k coincides with the one of the down quark state with $2k$ is simply due to the fact that (in modulus) the electric charge of the up quark is twice that of the down quark. Regarding the behavior of the first order transition line (solid line in the figure), we can observe three distinct regions. For $eB \lesssim 0.06$ GeV^2 the critical chemical potential μ_c depends only weakly on eB, showing just a slight decrease as the magnetic field gets increased. Then, in the region from $eB \sim 0.06$ GeV^2 to $eB \sim 0.2$ GeV^2, a much pronounced decrease of μ_c is observed. The behavior found in these two regions is common to both parameterizations in Fig. 4, and it has also been observed in other models like the local NJL model [16,22] and the Sakai-Sugimoto model [20]. This corresponds to the so-called "inverse magnetic catalysis" effect that occurs at finite chemical potential. Now, the situation for magnetic fields larger than $eB \sim 0.2$ GeV^2 turns out to depend on the chosen parametrization, as it has been anticipated from the analysis of Fig. 2. In the case of the parametrization P230ch it is observed that the decrease of μ_c continues with a rather steep slope, whereas for P260ch it is found that the curve $\mu_c(eB)$ becomes almost flat for $eB \gtrsim 0.2$ GeV^2. It should be noted that for no reasonable parametrization of the nonlocal NJL model we find a strong increase of μ_c with eB, as it is observed in the local NJL model [22]. Actually, we have checked that a qualitatively similar behavior as that found in Fig. 4 is also obtained for other nonlocal form factor shapes, such as Lorenztian-like functions.

3.2 Finite current quark mass

In the case of a finite current quark mass, the input parameters of the model are three, namely Λ, G and m_c. They can be set so as to reproduce the phenomenological values of the pion mass and decay constant, $m_\pi = 139$ MeV and $f_\pi = 92.4$ MeV, and some acceptable input value of the quark condensate at zero μ and B. As in the chital limit case, we consider the values $-\langle\bar{q}q\rangle^{1/3} = 230$ MeV and 260 MeV. The corresponding parametrizations are denoted as P230 and P260, respectively. For P230 one has $\Lambda = 677.8$ MeV, $G\Lambda^2 = 23.65$ and $m_c = 6.4$ MeV, whereas for P260 one has $\Lambda = 903.4$ MeV, $G\Lambda^2 = 17.53$ and $m_c = 4.6$ MeV.

As discussed in the previous subsection, once the input parameters have been fixed one can numerically solve the gap equation (15) for given values of the chemical potential and the magnetic field strength. As in the chiral limit case, taking a fixed value of eB, for $\mu = 0$ the system always lies in a phase **B** in which chiral symmetry is spontaneously broken (the absolute minimum of the thermodynamic potential occurs for a solution with a relatively large value of $\bar{\sigma}$). Then, if the chemical potential is increased, at some critical value $\mu = \mu_c$ the system undergoes a transition to a phase $\mathbf{A}_k$, in which $\bar{\sigma}$ jumps to a small value, indicating an approximate

restoration of chiral symmetry. This is shown in Fig. 5, where we quote the phase diagrams in the $eB-\mu$ plane corresponding to parametrizations P230 and P260.

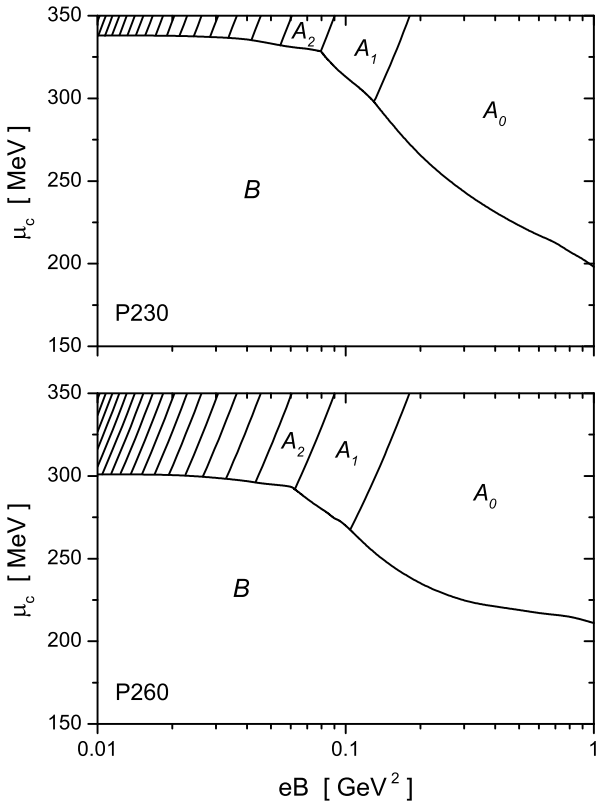

Fig. 5 Phase diagrams for the case of finite current quark masses. Upper and lower panels correspond to parametrizations P230 and P260, respectively.

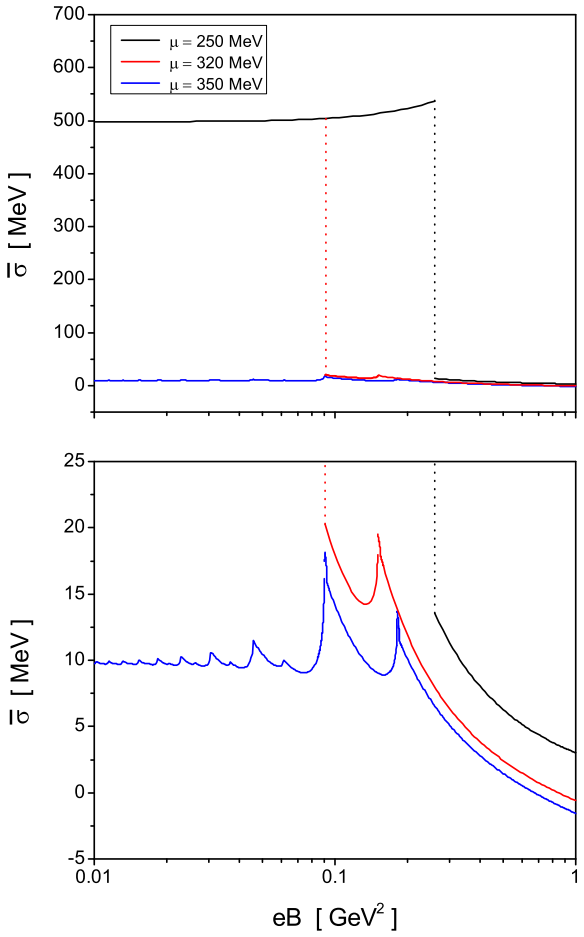

Fig. 6 $\bar{\sigma}$ as a function of the magnetic field for three representative values of the quark chemical potential. The results correspond to parametrization P230.

It can be seen that the phase structure is similar to that found in the chiral limit case. Inverse magnetic catalysis is found for finite μ, as the critical chemical potential decreases for increasing external magnetic field. In addition, it is found that the phase space region in which chiral symmetry is approximately restored is subdivided into many phases $\mathbf{A}_k$, $k = 0, 1, 2, \ldots$, which correspond to different population of the Landau levels. However, notice that in this case the value of the order parameter $\bar{\sigma}$ in the $\mathbf{A}_k$ phases is nonvanishing, therefore it can be used to signal not only the chiral restoration transition but also the van Alphen-de Haas transitions. This is illustrated in Fig. 6, where we show the behavior of $\bar{\sigma}$ as a function of eB for parametrization P230, taking three different fixed values of μ. In the upper panel, first order chiral restoration transitions are clearly seen for $\mu = 250$ MeV (black) and $\mu = 320$ MeV (red), from phase $\mathbf{B}$ to phases $\mathbf{A}_0$ and $\mathbf{A}_1$, respectively. For $\mu = 350$ MeV the system lies in the chiral restored region for all values of eB, therefore the value of $\bar{\sigma}$ remains close to zero (blue). Now, the vAdH transitions can be observed by looking at the lower panel of Fig. 6, in which we plot the same curves as in the upper panel using a different scale and concentrating on the region of small $\bar{\sigma}$. The curve corresponding to $\mu = 320$ MeV (red) shows, beyond the chiral restoration transition from the $\mathbf{B}$ phase to the $\mathbf{A}_1$ phase, a sharp peak denoting a vAdH transition from the $\mathbf{A}_1$ phase to the $\mathbf{A}_0$ one. A closer look indicates that there is a small discontinuity in the left hand side of this peak, indicating that the vAdH transition is in fact a first order one. Now, the curve corresponding to $\mu = 350$ MeV (blue) involves transitions between many $\mathbf{A}_k$ states, as can be seen from the phase diagram in Fig. 5. Each transition is characterized by the presence of a peak in $\bar{\sigma}(eB)$, the height of these peaks becoming smaller as the magnetic field gets decreased. As far as numerical calculations can show, these vAdH transition

are of first order, therefore they are represented by solid lines in Fig. 5. As discussed for the chiral limit case, the vAdH transitions correspond alternatively to the population of either a new level for the d-quark state or a new level for both the u and d-quark states. Therefore, they can be grouped into pairs, leading to the pattern observed in the lower panel of Fig. 6. It is worth noticing that the location of the vAdH transition curves in the $eB - \mu$ phase diagram shows just a slight shift with respect to those found in the chiral limit case, given by Eq. (19).

4 Conclusions

In the present work we have studied the behavior of cold and dense quark matter in the presence of an external homogeneous magnetic field. We have considered a two-flavor nonlocal NJL model, in which quark-antiquark currents include a Gaussian form factor.

It is find that for low values of the quark chemical potential μ the system lies in a phase $\mathbf{B}$ in which chiral symmetry is sponteneously broken, while at some critical value μ_c there is a first order phase transition in which this symmetry becomes approximately restored. The restored phase can be subdivided into many phases $\mathbf{A}_k$, characterized by the number of populated Landau levels for u and d-quark states.

In the chiral limit $m_c = 0$ it is seen that the van Alphen-de Haas transitions between $\mathbf{A}_k$ phases are of second order, and their effect shows up e.g. in the behaviour of the quark density. On the contrary, for finite quark masses these transitions are found to be of first order, though the corresponding jumps in the order parameter $\bar{\sigma}$ are rather tiny. Concerning the first order chiral restoration transition line, it is found that up to $eB \sim 0.2$ GeV^2 the critical chemical potential μ_c decreases with the magnetic field, showing an inverse magnetic catalysis effect. For larger values of eB the behaviour of μ_c becomes more or less flat, depending on the parametrization. In any case, for the considered parametrization range we do not find a significant growth of the critical chemical potential for large magnetic fields, as occurs in the case of the local NJL model.

Acknowledgements A. G. G. would like to acknowledge to CONICET for financial support under Grant No. PIP17-700.

References

1. Robert C. Duncan and Christopher Thompson. Formation of very strongly magnetized neutron stars - implications for gamma-ray bursts. *Astrophys. J. Lett.*, 392:L9, 1992.
2. D.P. Menezes, M. Benghi Pinto, S.S. Avancini, A. Perez Martinez, and C. Providencia. Quark matter under strong magnetic fields in the Nambu-Jona-Lasinio Model. *Phys. Rev. C*, 79:035807, 2009.
3. D.P. Menezes, M. Benghi Pinto, S.S. Avancini, and C. Providencia. Quark matter under strong magnetic fields in the su(3) Nambu-Jona-Lasinio Model. *Phys. Rev. C*, 80:065805, 2009.
4. John C Collins and Malcolm J Perry. Superdense matter: neutrons or asymptotically free quarks? *Physical Review Letters*, 34(21):1353, 1975.
5. Nicola Cabibbo and Giorgio Parisi. Exponential hadronic spectrum and quark liberation. *Physics Letters B*, 59(1):67–69, 1975.
6. Yoichiro Nambu and G. Jona-Lasinio. Dynamical Model of Elementary Particles Based on an Analogy with Superconductivity. I. *Phys. Rev.*, 122:345–358, 1961.
7. Yoichiro Nambu and G. Jona-Lasinio. Dynamical Model of Elementary Particles Based on an Analogy with Superconductivity. II. *Phys. Rev.*, 124:246–254, 1961.
8. S. M. Schmidt, D. Blaschke, and Yu. L. Kalinovsky. Scalar - pseudoscalar meson masses in nonlocal effective QCD at finite temperature. *Phys. Rev.*, C50:435–446, 1994.
9. G. Ripka. *Quarks bound by chiral fields: The quark-structure of the vacuum and of light mesons and baryons.* 1997.
10. D. Gomez Dumm, J. P. Carlomagno, and N. N. Scoccola. Strong-interaction matter under extreme conditions from chiral quark models with nonlocal separable interactions. *Symmetry*, 13:121, 2021.
11. V. P. Gusynin, V. A. Miransky, and I. A. Shovkovy. Catalysis of dynamical flavor symmetry breaking by a magnetic field in (2+1)-dimensions. *Phys. Rev. Lett.*, 73:3499–3502, 1994. [Erratum: Phys. Rev. Lett.76,1005(1996)].
12. G. S. Bali, F. Bruckmann, G. Endrodi, Z. Fodor, S. D. Katz, S. Krieg, A. Schafer, and K. K. Szabo. The QCD phase diagram for external magnetic fields. *JHEP*, 02:044, 2012.
13. G. S. Bali, F. Bruckmann, G. Endrodi, Z. Fodor, S. D. Katz, and A. Schafer. QCD quark condensate in external magnetic fields. *Phys. Rev.*, D86:071502, 2012.
14. D. Ebert, K. G. Klimenko, M. A. Vdovichenko, and A. S. Vshivtsev. Magnetic oscillations in dense cold quark matter with four fermion interactions. *Phys. Rev.*, D61:025005, 2000.
15. D. Ebert and K. G. Klimenko. Quark droplets stability induced by external magnetic field. *Nucl. Phys.*, A728:203–225, 2003.
16. Tomohiro Inagaki, Daiji Kimura, and Tsukasa Murata. Four fermion interaction model in a constant magnetic field at finite temperature and chemical potential. *Prog. Theor. Phys.*, 111:371–386, 2004.
17. Jorn K. Boomsma and Daniel Boer. The Influence of strong magnetic fields and instantons on the phase structure of the two-flavor NJL model. *Phys. Rev.*, D81:074005, 2010.
18. Gabriel N. Ferrari, Andre F. Garcia, and Marcus B. Pinto. Chiral Transition Within Effective Quark Models Under Magnetic Fields. *Phys. Rev.*, D86:096005, 2012.
19. Efrain J. Ferrer and Vivian de la Incera. Magnetism in Dense Quark Matter. *Lect. Notes Phys.*, 871:399–432, 2013.
20. Florian Preis, Anton Rebhan, and Andreas Schmitt. Inverse magnetic catalysis in dense holographic matter. *JHEP*, 03:033, 2011.

21. Sidney S. Avancini, Debora P. Menezes, Marcus B. Pinto, and Constanca Providencia. The QCD Critical End Point Under Strong Magnetic Fields. *Phys. Rev.*, D85:091901, 2012.
22. Pablo G. Allen and Norberto N. Scoccola. Quark matter under strong magnetic fields in SU(2) NJL-type models: parameter dependence of the cold dense matter phase diagram. *Phys. Rev.*, D88:094005, 2013.
23. A. G. Grunfeld, D. P. Menezes, M. B. Pinto, and N. N. Scoccola. Phase structure of cold magnetized quark matter within the SU(3) NJL model. *Phys. Rev.*, D90(4):044024, 2014.
24. Pablo G. Allen, Valeria P. Pagura, and Norberto N. Scoccola. Cold magnetized quark matter phase diagram within a generalized SU(2) NJL model. *Phys. Rev.*, D91(11):114024, 2015.
25. Pablo G. Allen, Ana G. Grunfeld, and Norberto N. Scoccola. Magnetized color superconducting cold quark matter within the $SU(2)_f$ NJL model: A novel regularization scheme. *Phys. Rev.*, D92(7):074041, 2015.
26. Tanumoy Mandal and Prashanth Jaikumar. Effect of strong magnetic field on competing order parameters in two-flavor dense quark matter. *Adv. High Energy Phys.*, 2017:6472909, 2017.
27. Tanumoy Mandal, Prashanth Jaikumar, and Sanatan Digal. Chiral and Diquark condensates at large magnetic field in two-flavor superconducting quark matter. 2009.
28. Sh. Fayazbakhsh and N. Sadooghi. Color neutral 2SC phase of cold and dense quark matter in the presence of constant magnetic fields. *Phys. Rev.*, D82:045010, 2010.
29. M. Coppola, P. Allen, A. G. Grunfeld, and N. N. Scoccola. Magnetized color superconducting quark matter under compact star conditions: Phase structure within the SU(2)f NJL model. *Phys. Rev.*, D96(5):056013, 2017.
30. V. P. Pagura, D. Gomez Dumm, S. Noguera, and N. N. Scoccola. Magnetic catalysis and inverse magnetic catalysis in nonlocal chiral quark models. *Phys. Rev.*, D95(3):034013, 2017.
31. D. Gómez Dumm, M. F. Izzo Villafañe, and N. N. Scoccola. Neutral meson properties under an external magnetic field in nonlocal chiral quark models. *Phys. Rev.*, D97(3):034025, 2018.
32. D. Gómez Dumm, M. F. Izzo Villafañe, and N. N. Scoccola. Properties of magnetized neutral pions at zero and finite temperature in nonlocal chiral quark models. *Phys. Rev.*, D101(11):116018, 2020.
33. D. Gómez Dumm, M. F. Izzo Villafañe, S. Noguera, V. P. Pagura, and N. N. Scoccola. Strong magnetic fields in nonlocal chiral quark models. *Phys. Rev.*, D96(11):114012, 2017.
34. S Noguera and NN Scoccola. Nonlocal chiral quark models with wavefunction renormalization: Sigma properties and π- π scattering parameters. *Physical Review D*, 78(11):114002, 2008.
35. D Gomez Dumm, S Noguera, and NN Scoccola. Pion radiative weak decays in nonlocal chiral quark models. *Physics Letters B*, 698(3):236–242, 2011.
36. D Gomez Dumm, AG Grunfeld, and NN Scoccola. Covariant nonlocal chiral quark models with separable interactions. *Physical Review D*, 74(5):054026, 2006.
37. Claude Bloch. On field theories with non-localized interaction. *Kong. Dan. Vid. Sel. Mat. Fys. Med.*, 27N8(8):1–55, 1952.